Journal of Alloys and Compounds 1056 (2026) 186613

Contents lists available at ScienceDirect

Journal of Alloys and Compounds

journal homepage: www.elsevier.com/locate/jalcom

A robust lithium magnesium silicate composite electrolyte with enhanced ionic conductivity toward high-performance solid-state lithium metal batteries

Panpan Dong [a,*], Shangzhang Yu [b], Xuemeng Gan [a], Qilin He [a], Xiaojie Zheng [b], He Lin [a], Xiaoping Wang [c], Qiao Lin [a], Liangjie Gu [a], Qingsong Zhang [c,*], Weiqing Yang [a,*]

[a] Research Institute of Frontier Science, Key Laboratory of Advanced Technologies of Materials (Ministry of Education), School of Materials Science and Engineering, Southwest Jiaotong University, Chengdu, Sichuan 610031, China
[b] School of Chemistry, Southwest Jiaotong University, Chengdu, Sichuan 610031, China
[c] State Key Laboratory of Advanced Separation Membrane Materials, School of Materials Science and Engineering, Tiangong University, Tianjin 300387, China

ARTICLE INFO

Keywords:
Lithium magnesium silicate
Poly(ethylene) oxide
Ion transport
Thermal stability
Solid-state lithium metal batteries

ABSTRACT

Poly(ethylene) oxide (PEO)-based electrolytes have been widely studied for solid-state lithium batteries due to their good flexibility and compatibility with lithium metal, while their ionic conductivity and thermal stability still need to be further improved. Herein, we report a PEO-based composite electrolyte (denoted as PTLL) reinforced with thermoplastic polyurethane and two-dimensional lithium magnesium silicate (LMS, $Li_2Mg_2Si_3O_9$) for solid-state lithium metal batteries. The incorporation of LMS and the polymer blend effectively reduces the crystallinity of PEO matrix while significantly enhancing the mechanical strength of PTLL electrolyte. Additionally, the PTLL exhibits a high ionic conductivity (2.48×10^{-4} S cm^{-1} at 30 °C), enhanced thermal stability (150 °C), and a higher onset oxidative voltage (>4.2 V) when compared to conventional PEO electrolytes (1.06×10^{-5} S cm^{-1} at 30 °C; onset oxidative voltage at 3.83 V). Furthermore, symmetrical lithium cell with the robust PTLL electrolyte demonstrates good cycling stability up to 800 h with a stable polarization voltage, indicating good compatibility of PTLL with lithium metal. As a result, Li/$LiFePO_4$ cell with PTLL electrolyte exhibits a much higher specific capacity of 165.5 mAh g^{-1} at 0.1 C and better reversibility at 0.5 C with a high average Coulombic efficiency > 99.8 % at 60 °C than those of conventional PEO electrolyte. Moreover, the PTLL-based Li/NCM811 cell enables a high specific capacity of 155.4 mAh g^{-1} at 0.1 C. This work also provides a promising strategy for designing advanced composite electrolytes toward high-performance solid-state lithium metal batteries.

1. Introduction

With the growing global demand for sustainable energy and electric vehicles, the development of energy storage systems featuring high energy density and enhanced safety has become a critical focus of scientific research and industrial applications [1]. Lithium-ion batteries (LIBs), as the current mainstream electrochemical energy storage technology, are widely used in portable electronic devices and electric vehicles owing to their high energy density and long cycle life [2,3]. However, conventional LIBs use flammable organic liquid electrolytes, posing safety risks such as leakage, combustion, and explosion, which severely limit their applications in next-generation scenarios requiring high safety standards. To overcome these limitations, solid-state lithium metal batteries (SSLMBs), which replace liquid electrolytes with solid ones [4,5], are regarded as one of the most promising next-generation battery technologies, attracting extensive attention because of their inherent safety and potential for higher energy density [6,7].

Solid electrolytes play a crucial role in maintaining effective ion transport and good safety of SSLMBs during operating, therefore, much efforts have been devoted to improving the ionic conductivity and stability of electrolytes in SSLMBs. So far, the commonly reported solid electrolytes can be classified into organics [8,9] (e.g., solid polymers, gel electrolytes), inorganics [10–12] (e.g., oxides, sulfides, and nitrides), organic-inorganic composites [13] (e.g., polymer with ceramics), and

* Corresponding authors.
E-mail addresses: panpan.dong@swjtu.edu.cn (P. Dong), zqs8011@163.com (Q. Zhang), wqyang@swjtu.edu.cn (W. Yang).

https://doi.org/10.1016/j.jallcom.2026.186613
Received 12 November 2025; Received in revised form 21 January 2026; Accepted 2 February 2026
Available online 4 February 2026
0925-8388/© 2026 Elsevier B.V. All rights are reserved, including those for text and data mining, AI training, and similar technologies.

some unconventional electrolytes [14,15] (e.g., halides, metal-organic frameworks). Among these solid electrolytes, polymer-based solid electrolytes are considered one of the most promising systems for large-scale application owing to their good flexibility, easy processability, and good compatibility with electrodes in SSLMBs [16]. Among various polymer electrolytes, poly(ethylene oxide) (PEO) has been widely studied as promising candidate for SSLMBs owing to its strong ability to dissociate lithium salts, good segmental mobility, and relative stability against lithium metal [17–19]. The ether oxygen atoms in the molecular structure of PEO can coordinate with lithium ions, facilitating their migration and thus providing ion conduction pathways. However, conventional PEO-based electrolytes suffer from several inherent drawbacks that severely limit their practical applications in SSLMBs. First, the high crystallinity of PEO results in low ionic conductivity at room temperature (10^{-6} to 10^{-8} S cm^{-1}), which is less than practical application requirements. Second, PEO-based electrolytes lack sufficient mechanical strength to effectively suppress lithium dendrite growth, leading to failure of batteries for long cycling. Moreover, PEO electrolytes exhibit a relatively low onset oxidative voltage (typically below 4.0 V) because of poor oxidation resistance of PEO [20,21], rendering them incompatible with high-voltage cathode materials (e.g., $LiCoO_2$, $LiNi_xCo_yMn_zO_2$), which are crucial for achieving high energy density.

To address the above-mentioned challenges of conventional PEO electrolytes, much efforts have been conducted to designing PEO-based hybrid solid electrolytes [22,23]. Some inert ceramic fillers, such as Al_2O_3 [24], SiO_2 [25], and ZrO_2 [26], have been previously reported to enhance the ion transport and mechanical strength of PEO-based composite electrolytes. Later, active fillers, such as Li_3N [27], LLZO [28], LLZTO [29,30], and LATP [31], have been selected to further improve the ionic conductivity as well as oxidative stability of PEO electrolytes, resulting from the extra lithium-ion conduction pathways as well as wide electrochemical window of these ceramic fillers. Additionally, novel fillers, such as metal–organic frameworks [32,33] and covalent organic frameworks [34], have been considered functional additives to effectively enhance lithium-ion transport in PEO-based composite electrolytes, which is attributed to strong Lewis-acid interaction between lithium salt anions and these fillers. Although advances have been made in PEO-based electrolytes, the synergistic enhancement of ionic conductivity, mechanical strength, and electrochemical stability remains elusive.

Recently, two-dimensional (2D) materials have been reported as functional fillers for solid composite electrolytes because of their unique layered structures and ion transport properties [35,36]. For example, Li et.al reported a novel PEO-based electrolyte with 2D CeF_3 nanoplates for SSLMBs with long cycling life [37]. Owing to the interaction between CeF_3 nanoplates and PEO, the composite electrolyte exhibits reduced crystallinity and thus enhanced ion transport, leading to much improved ionic conductivity and enhanced electrochemical stability. Nonetheless, this PEO composite electrolyte with CeF_3 still shows a low lithium-ion transference number (<0.4), which may result in uneven lithium deposition and thus lithium dendrite growth during cycling. Lithium magnesium silicate (LMS, $Li_2Mg_2Si_3O_9$), as a layered silicate material, possesses regular channel structures and abundant lithium sites, which shows great potential for facilitating rapid Li^+ ion transport. Very recently, LMS layer has been reported as an active filler for PVDF-HFP-based solid electrolytes to achieve high ionic conductivity and lithium-ion transference number [38,39]. The incorporation of LMS can disrupt the orderly arrangement of polymer chains, promote lithium salt dissociation, as well as enhance electrochemical stability of PVDF-HFP electrolytes. Nevertheless, the current understanding of functional mechanism of 2D LMS nanosheets in PEO-based electrolytes is still limited, which needs further fundamental study.

Herein, we design a PEO-based composite electrolyte (denoted as PTLL), reinforced with thermoplastic polyurethane and 2D lithium magnesium silicate to achieve synergistic enhancement. We systematically investigate the microstructure, ionic transport, and electrochemical property of the PTLL composite electrolyte, as well as evaluate its practical application in high-performance solid-state lithium metal batteries. Compared with conventional PEO electrolytes, the robust PTLL electrolyte exhibits much enhanced ionic conductivity (2.48×10^{-4} S cm^{-1} at 30 °C), a higher lithium-ion transference number (0.42), good thermal stability (up to 150 °C), and a higher onset oxidative voltage (4.21 V). Beneficial in the facilitated Li^+ ion transport of PTLL electrolyte, symmetric Li/Li cell with PTLL electrolyte exhibits good cycling stability up to 800 h with a stable polarization voltage. Moreover, the PTLL-based Li/LFP and Li/NCM811 cells exhibit much enhanced cycling stability and rate capability. This study not only develops a high-performance composite electrolyte but also provides strategy for designing next-generation solid-state lithium metal batteries.

2. Experimental

2.1. Materials and chemicals

Lithium bis(trifluoromethanesulfonyl) imide (LiTFSI, ≥99.9 %), poly (ethylene) oxide (PEO, M_v=40,000 g mol^{-1}), acetonitrile (≥99.5 %, ACS reagent), *N*,*N*-dimethylformamide (DMF, ≥99 %), 1-butyl-1-methylpyrrolidinium bis(trifluoromethanesulfonyl)imide (Pyr_{14}TFSI, ≥99 %), and *N*-methylpyrrolidone (NMP, ≥99 %) was purchased from Aladdin. Thermoplastic urethane (TPU, M_w=3000 g mol^{-1}) was purchased from BASF. Lithium magnesium silicate (LMS, $Li_2Mg_2Si_3O_9$) was provided by Shijiazhuang Zixinjia Technology Co., Ltd. $LiFePO_4$ (LFP), $LiNi_{0.8}Co_{0.1}Mn_{0.1}O_2$ (NCM811), Super-C45, and polyvinylidene difluoride (PVDF) were purchased from Canrd. Lithium metal (≥99.9 %, diameter: 15.6 mm, thickness: 450 μm) was purchased from NEWARE. Prior to use, LiTFSI and PEO were dried at 120 °C and 60 °C, respectively, overnight under vacuum. All other materials and chemicals were used as-received.

2.2. Preparation of PL, PTL, and PTLL electrolytes

In this work, the molar ratio of [EO]:[Li] was controlled as 16:1. PL electrolyte was prepared by mixing PEO (0.6667 g) with LiTFSI (0.2719 g) in acetonitrile (9.5 mL). The obtained solution was then poured into a PTFE dish and dried at room temperature overnight and further dried at 50 °C under vacuum to evaporate solvent. The obtained sample was cut into a disk with a diameter of 19 mm. PTL and PTLL electrolytes were prepared using the same method. For PTL electrolyte, TPU (0.1667 g) was first dissolved in DMF (1.5 mL). The obtained TPU/DMF solution was then mixed with PEO (0.5 g) and LiTFSI (0.2 g) in acetonitrile (8 mL). For PTLL electrolyte, different amounts of LMS (5, 10, 15 wt%) based on PEO+LiTFSI+TPU+LMS was added into the above solution and mixed overnight. The 2D LMS nanosheets were first ground before adding to polymer electrolyte solution for better dispersion. The obtained electrolyte was further hot-pressed at 60 °C for 1 min with the pressure of 5 MPa. The thickness of electrolyte was ~200 μm. The specific compositions of PTLL electrolyte are shown in Table S1. In this work, the PTLL electrolyte refers to PEO/TPU with 5 wt% of LMS unless otherwise stated. All preparation processes were operated in an argon-filled glove box with both moisture and oxygen level of < 0.01 ppm.

2.3. Characterization methods

Scanning electron microscopy (SEM) morphology and energy dispersive X-ray spectroscopy (EDS) mapping were observed with a HITACHI SU8010. All electrolyte samples were coated with a platinum layer for 50 s under a current of 30 mA. X-ray diffraction (XRD) was performed with a SmartLab from 5 to 40 ° with a scan rate of 2 ° min^{-1}. Transmission electron microscopy (TEM) measurement were carried out using a JEOL JEM-2100F microscope. Fourier transform infrared (FT-IR)

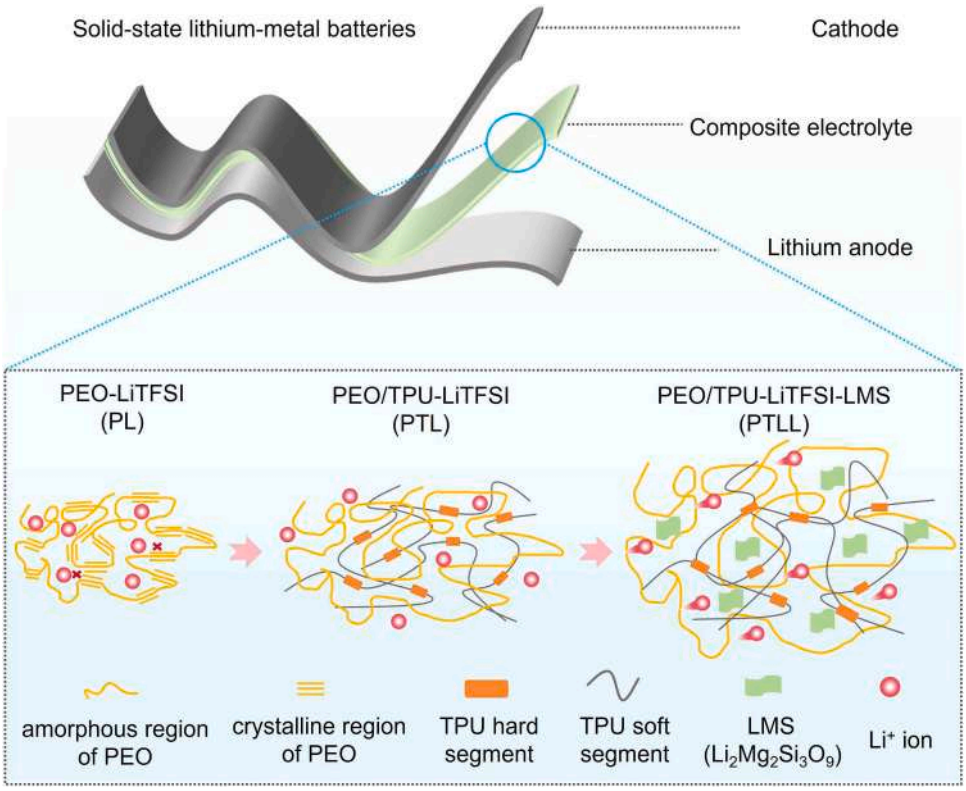


Fig. 1. Schematic design of the PTLL composite electrolyte for solid-state lithium metal batteries.

spectroscopy was collected using a Nicolet IS5 FT-IR Spectrometer (Thermo Scientific) in a range of 600–4000 cm^{-1} with a resolution of 4 cm^{-1}. Raman spectroscopy was collected by a LabRam HR Evolution (Thermo Fischer DXR) equipped with a 532 nm excitation laser in a scan range of 200–2000 cm^{-1}. Tensile strength of electrolyte was carried out using an Instron 4466 Universal test machine with a load of 4 N and a tensile rate of 5 mm min^{-1}.

Electrochemical impedance spectroscopy (EIS) measurements were performed on a potentiostat (Squidstat Plus, Ai Admiral Instruments) in a frequency range from 2 MHz to 10 mHz with an AC oscillation amplitude of 10 mV. Ionic conductivity was measured by sandwiching electrolyte between two stainless steel electrodes, i.e., SS/electrolyte/SS cell. EIS measurement of the cell was tested from 30 to 80 °C. Prior to the EIS measurements, the cells were kept at each test temperature for 30 min to reach thermal equilibrium. The ionic conductivity (σ) was calculated via the following Eq. (1):

$$\sigma = L/(R \times S) \tag{1}$$

where L, R, and S refer to the thickness of electrolyte, the ohmic resistance, and the area of electrolyte. The activation energy (E_a) for Li^+ ion transport was determined according to the Eq. (2):

$$\sigma = \sigma_0 \exp^{(E_a/kT)} \tag{2}$$

Where σ refers to the ionic conductivity at temperature T, σ_0 refers to the prefactor, and k refers to Boltzmann constant (8.617 × 10^{-5} eV K^{-1}).

The lithium-ion transference number (t_{Li}^+) was measured using a cell configuration of Li/electrolyte/Li at 60 °C with a D.C. polarization voltage of 10 mV. EIS tests were performed before and after polarization process. The t_{Li}^+ was calculated by Bruce-Vincent method via the following Eq. (3):

$$t_{Li^+} = I_{ss}(\Delta V - I_o R_o)/I_o(\Delta V - I_{ss}R_{ss}) \tag{3}$$

where ΔV is the D.C. polarization voltage; I_o and I_{ss} are the initial and steady-state current, respectively; R_o and R_{ss} are the interfacial resistance before and after polarization, respectively.

Linear sweep voltammetry (LSV) measurement was performed under a scan rate of 0.5 mV s^{-1} from open circuit voltage to 6 V vs. Li/Li^+ with a cell configuration of SS/electrolyte/Li at 60 °C. Li plating and stripping behavior of electrolyte was measured using symmetric Li/Li cells at a current density of 0.1 mA cm^{-2} and 0.1 mAh cm^{-2} from −4.9 to 4.9 V vs. Li/Li^+ at 60 °C. To improve the interfacial compatibility, 5 μL of liquid electrolyte composed of 1 M LiTFSI in Pyr_{14}TFSI was added between lithium metal and electrolyte. All cells were rested 3 h at 60 °C before testing.

2.4. Battery measurements

Coin cells (CR2032 type, NEWARE) were assembled by sandwiching polymer electrolyte between LFP (or NCM811) cathode and Li metal anode. LFP electrode slurry was prepared by uniformly mixing LFP with Super-C45 and PVDF binder at a weight ratio of 7:2:1 in NMP solution. The obtained slurry was then coated on an aluminum current collector with an active materials mass loading of 1.2–1.5 mg cm^{-2}. The electrode was dried at 90 °C for 12 h under vacuum and punched into round shape with a diameter of 12 mm. The galvanostatic charge/discharge measurements of Li/LFP cells were carried out between 2.8 and 4.0 V vs. Li/Li^+ at 30 and 60 °C using a battery cycler (MHW-100–2–160CH, NEWARE). The Li/NCM811 cells were tested between 3.0 and 4.2 V vs. Li/Li^+ at 60 °C. The PTLL-based full cell (graphite/LFP) was assembled by pairing LFP cathode with graphite anode (Canrd Technology Co., Ltd.). The diameter of graphite anode is 14 mm with the N/P ratio of 2. The PTLL-based full cell was measured at 0.01 C and 0.1 C at 60 °C under thee voltage window between 2.0 and 3.65 V vs. Li/Li^+. To improve the interfacial compatibility between electrode and electrolyte, 5 μL of liquid electrolyte (1 M LiTFSI in Pyr_{14}TFSI) was added between cathode and polymer electrolyte for the above cells. All cells were rested for 3 h at 60 °C before testing. 1 C was defined as 170 mA g^{-1} and

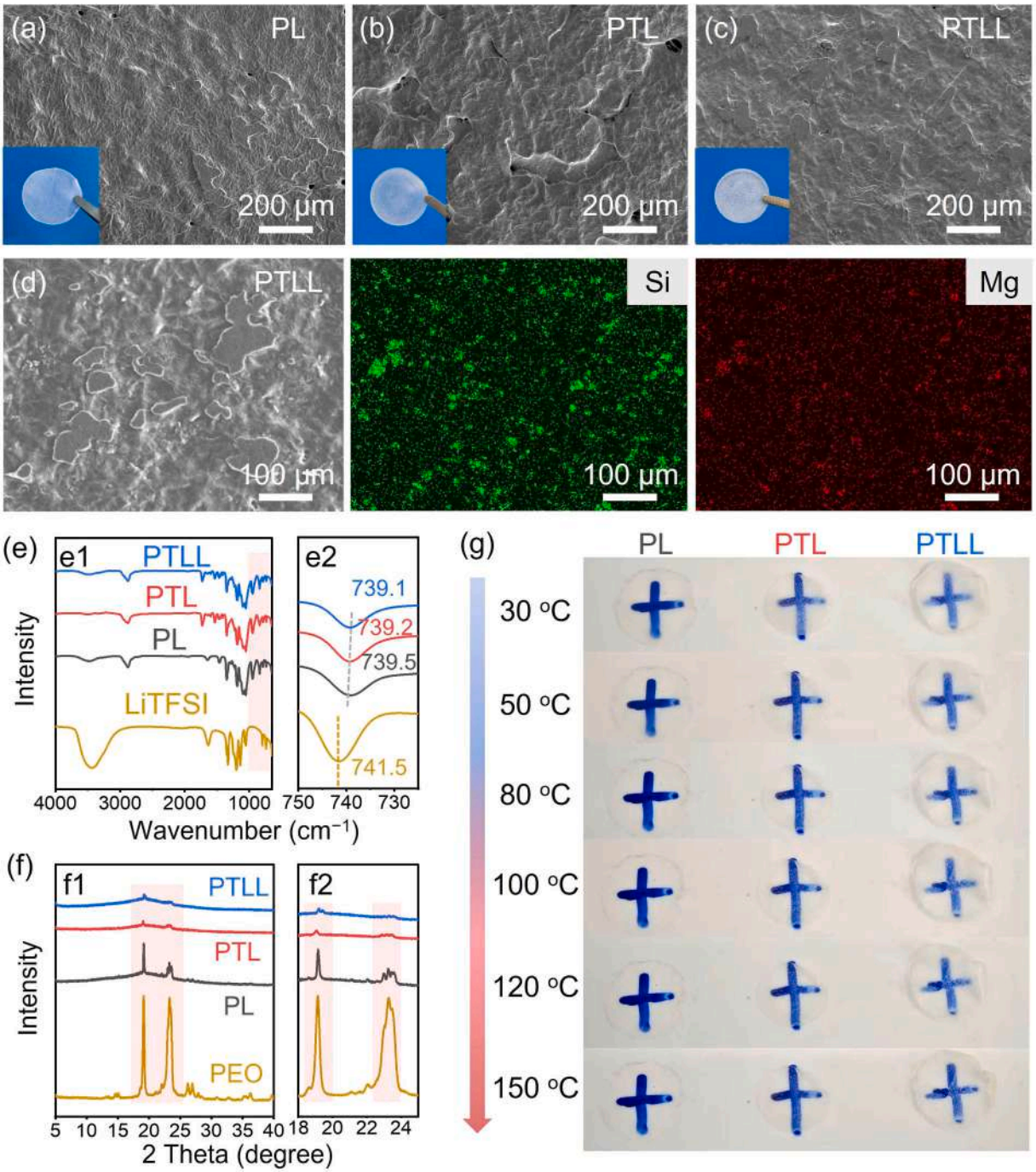


Fig. 2. Characterization of the composite electrolytes. SEM images of (a) PL, (b) PTL, and (c) PTLL electrolytes. The insets are optical images of electrolytes. (d) SEM/EDS mapping of PTLL electrolyte. PTLL refers to PTLL with 5 wt% of LMS in the composite electrolyte. (e) FT-IR spectra of LiTFSI, PL, PTL, and PTLL electrolytes. (f) XRD patterns of PEO, PT, PTL, and PTLL electrolytes. (g) Thermal stability of PL, PTL, and PTLL electrolytes at various temperatures ranging from 30 to 150 °C.

200 mA g^{-1} for Li/LFP (graphite/LFP) cells and Li/NCM811 cells, respectively.

3. Results and discussion

3.1. Preparation and characterization of PTLL electrolyte

The structural design concept of PTLL composite electrolyte is illustrated in Fig. 1a. The pristine PEO-based electrolyte exhibits high crystallinity, which strongly restricts the segmental motion of polymer chains and impedes the migration of lithium ions, leading to low ionic conductivity. To address this issue, thermoplastic polyurethane (TPU) was introduced into PEO matrix. The amorphous domain of TPU effectively reduces the crystallinity of PEO while significantly enhancing the mechanical strength of the electrolyte. Furthermore, two-dimensional lithium magnesium silicate (LMS, $Li_2Mg_2Si_3O_9$) nanosheets with an average diameter of ~26 nm and thickness of ~1 nm (Fig. S1) were incorporated in PTLL as functional fillers. The LMS nanosheets were supposed to not only suppress polymer crystallization but also provide abundant Lewis acid sites (Mg^{2+}) on surface that can interact with both polymer chains and anions, facilitating Li^+ dissociation and transport.

As shown in Fig. 2a–c, all electrolytes exhibit compact and smooth surfaces after hot press based on the SEM images. In the presence of TPU and LMS, the PTLL composite electrolyte displays a dense and uniform

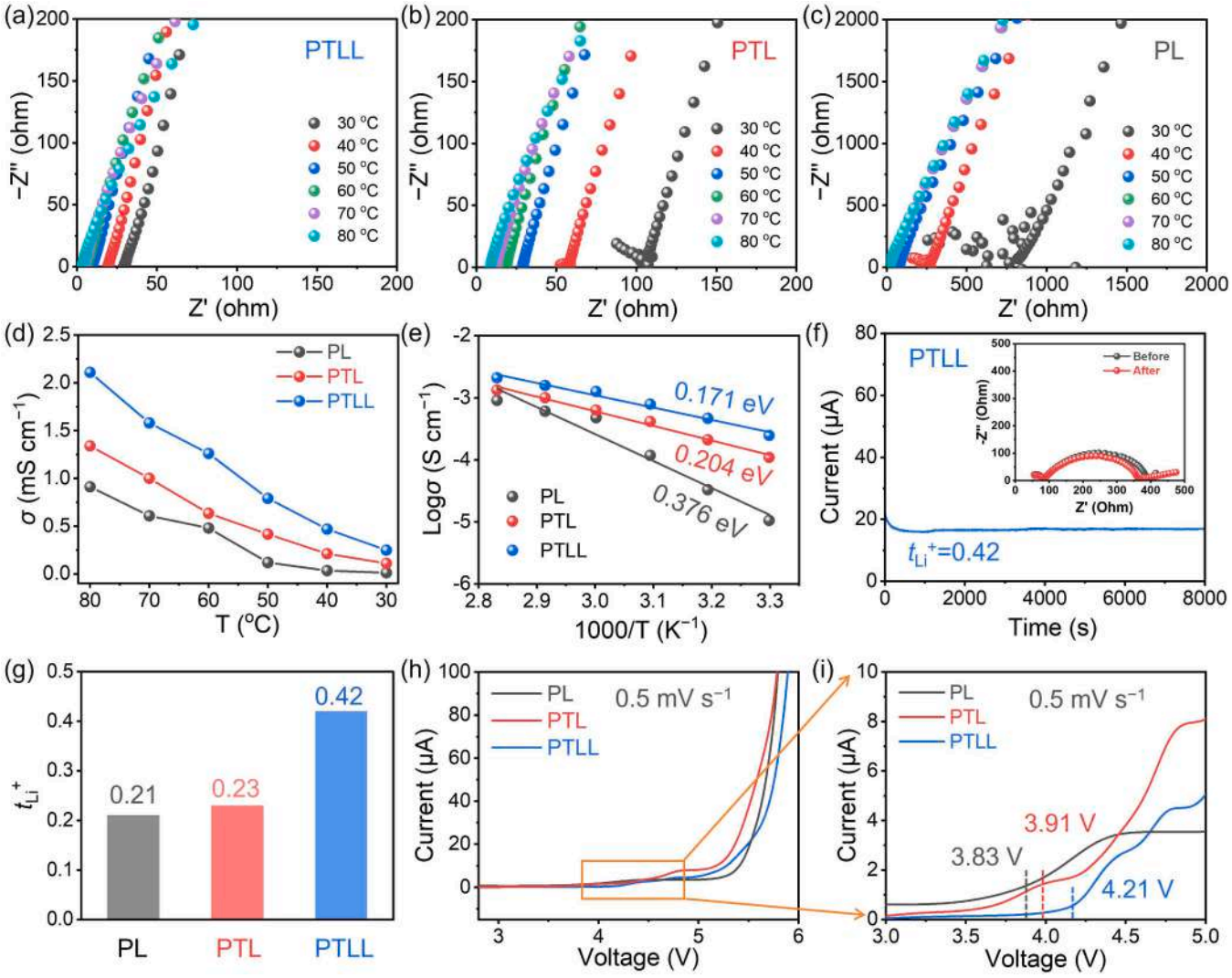


Fig. 3. Electrochemical properties of PTLL electrolyte. Nyquist plots of (a) PTLL, (b) PTL, and (c) PL electrolytes at various temperatures from 30 to 80 °C. (d,e) Comparison of the ionic conductivity of PTLL, PTL, and PL electrolytes. (f) Current–time curve and Nyquist plots before and after polarization of PTLL electrolyte at 60 °C. (g) Lithium-ion transference number (t_{Li}^+) of PL, PTL, and PTLL electrolytes. (h) LSV curves and (i) zoomed-in LSV curves of PL, PTL, and PTLL electrolytes at a scan rate of 0.5 mV s^{-1} at 60 °C.

morphology without visible cracks or pinholes. Additionally, PTLL electrolyte shows homogeneous distribution of Si and Mg elements as shown in Fig. 2d, suggesting uniform dispersion of LMS nanosheets in polymer matrix. This homogeneous distribution is critical for constructing continuous ion-conduction pathways along the filler-polymer interfaces, which contributes significantly to the enhancement of overall ionic conductivity. PTLL electrolyte shows agglomeration (Fig. S2) with the increased amount of LMS nanosheets (15 wt%), which might affect continuous ion conduction.

To investigate the effect of LMS nanosheets on the solvation structure of LiTFSI in PTLL electrolyte, we performed FT-IR spectroscopy (Figs. 2e and S3). As shown in Fig. 2e, LiTFSI salt shows a peak at 741.5 cm^{-1} that can be assigned to the bending of sulfonyl group of $TFSI^-$ anion. The lower the wavenumber of this sulfonyl group peak, the higher fraction of free and dissociated $TFSI^-$ anions in electrolyte. For PL electrolyte, the peak of sulfonyl group shifts to a lower wavenumber at 739.5 cm^{-1}, suggesting the dissociation of LiTFSI in PEO. In the presence of TPU, the PTL shows a peak shift to a much lower wavenumber (739.2 cm^{-1}) than that of PL, which is probably due to the interactions between sulfonyl group of $TFSI^-$ anion and polar segments such as NH, C═O, and C–O–C of TPU [40]. Moreover, compared with PL and PTL, the PTLL electrolyte shows a distinct shift of sulfonyl group peak to a much lower wavenumber (739.1 cm^{-1}), indicating more dissociated LiTFSI in PTLL electrolyte in the presence of both TPU and LMS. This result is mainly attributed to the extra interaction between Lewis acid sites on LMS and sulfonyl group of $TFSI^-$ anion [38], which effectively weakens the coordination between Li^+ and $TFSI^-$ anion. This is also confirmed by the Raman spectroscopy of polymer electrolytes (Fig. S4). The Raman spectra in the region of 730–760 cm^{-1} were deconvoluted to distinguish between "free" $TFSI^-$ anions and those in contact ion pairs (CIPs) or aggregates (AGGs) [41]. The PTLL electrolyte exhibits the lowest proportion of "free" $TFSI^-$ anions (8.5 %) compared with PL (18.7 %) and PTL (17.6 %) electrolytes, indicating the anions are immobilized by LMS nanosheets, which facilitates fast Li^+ transport.

The crystal structures of PTLL, PTL, and PL electrolytes were further investigated by XRD measurement (Fig. 2f and S5). As shown in Fig. 2f, PEO shows two diffraction peaks at $2\theta = 19.2°$ and 23.4° that correspond to the semi crystalline nature of PEO chain [42]. PTL electrolyte shows much reduced intensity of PEO peaks, which might attribute to the interaction among LiTFSI, PEO, and TPU as previously reported [40]. Moreover, the PTLL electrolyte shows the lowest crystallinity than that of PL and PTL electrolytes, indicating more amorphous phase of PEO in PTLL electrolyte. The effective reduction in PEO crystallization peaks of PTLL electrolyte demonstrates that TPU and LMS nanosheets

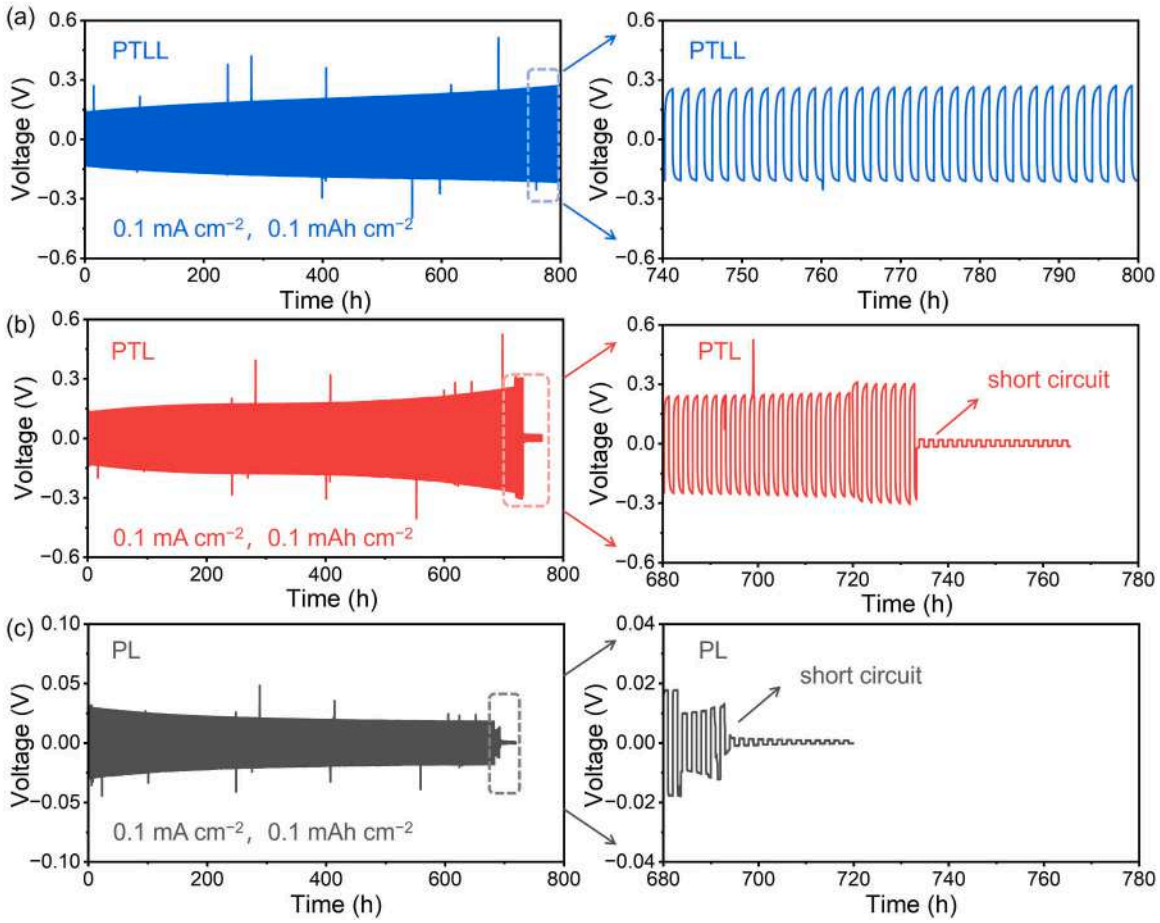


Fig. 4. Lithium plating/stripping measurement of PTLL electrolyte. Voltage–time profiles of symmetrical Li/Li cells with (a) PTLL, (b) PTL, and (c) PL electrolytes at a current density of 0.1 mA cm^{-2} and 0.1 mAh cm^{-2} at 60 °C.

act synergistically to disrupt polymer chain ordering. TPU segments introduce amorphous domains in polymer matrix, while LMS nanosheets further provide physical constraints of PEO chain, which can expand ion-conducting pathways and promote the motion of lithium ions in PTLL electrolyte. Moreover, we further evaluated the thermal stability and tensile strength of various electrolytes. The PTLL electrolyte still maintains its original shape even at a high temperature of 150 °C (Fig. 2g), while PL and PTL electrolytes undergo irreversible deformation at 80 °C due to the loss of mechanical integrity upon melting. The tensile test results (Fig. S6) show that PTLL exhibits an improved tensile strength of 1.21 MPa than that of PL (0.95 MPa) and PTL (1.06 MPa) electrolytes, which is attributed to the rigid LMS framework and interaction between TPU and PEO chains.

3.2. Ion transport of PTLL electrolyte

The ionic conductivity of the prepared electrolytes (PTLL, PTL, and PL) was evaluated by EIS measurement at various temperatures ranging from 30 to 80 °C (Fig. 3a–c). PTLL electrolyte achieves a higher ionic conductivity of 2.48×10^{-4} S cm^{-1} at 30 °C than PTL (1.09×10^{-4} S cm^{-1}) and PL (1.06×10^{-5} S cm^{-1}) electrolytes. The ionic conductivity of various electrolytes follows the decreasing order in Fig. 3d: PTLL > PTL > PL. This order is consistent with the decreasing order of crystallinity degree in Fig. 2f, indicating promoted Li^+ transport in PTLL electrolyte. To further study temperature-dependent ion mobility of PTLL electrolyte, we calculated activation energy from Arrehenius plots of ionic conductivity (Fig. 3e). PTLL electrolyte shows a lower activation energy of 0.171 eV than PTL (0.204 eV) and PL (0.376 eV), which is due to facile ion diffusion in amorphous polymer matrix of PTLL in the presence of TPU and LMS nanosheets. Additionally, the Lewis acid–base interactions between LMS and $TFSI^-$ anions weaken the ion pairing of LiTFSI salt, providing more free Li^+ ions and facilitating their migration in PTLL network. However, with the increased amount of LMS nanosheets, PTLL-10 and PTLL-15 electrolytes show gradually decreased ionic conductivity (Fig. S7), which is probably attributed to agglomeration of LMS in PTLL network as shown in Fig. S2. Therefore, in the following section, we select PTLL with 5 wt% of LMS as the model PTLL electrolyte because of its higher ionic conductivity compared with other PTLL electrolytes.

To further study the ion transport of PTLL electrolyte, we measured lithium-ion transference number (t_{Li^+}) at 60 °C using the Bruce-Vincent method. The Li-ion transference number of various electrolytes follows the decreasing order of PTLL (0.42) > PTL (0.23) > PL (0.21) (Fig. 3f, g, and S8). For PTLL electrolyte, $TFSI^-$ anions are immobilized by positive metal sites of LMS nanosheets surface via Lewis acid–base interactions, leading to a relatively high Li-ion transference number. In contrast, the PL and PTL electrolytes show low Li-ion transference number, which is mainly attributed to the strong coordinated Li^+ ions by polymer chain and thus $TFSI^-$ anions move freely in polymer matrix. We further evaluated the electrochemical stability of these three electrolytes. All three electrolytes exhibit oxidation stability beyond 4.5 V according to the full-scale LSV curevs from open circuit voltage to 6 V (Fig. 3h). However, a closer examination of the onset decomposition region reveals significant differences (Fig. 3i), which has been typically overlooked. PL electrolyte shows an onset oxidation potential of 3.83 V, which is owing to the decomposition of PEO chain [43]. Incorporating TPU and LMS nanosheets significantly increases the onset oxidation potential of the PTLL electrolyte to 4.21 V, compared to 3.83 V for the PL electrolyte.

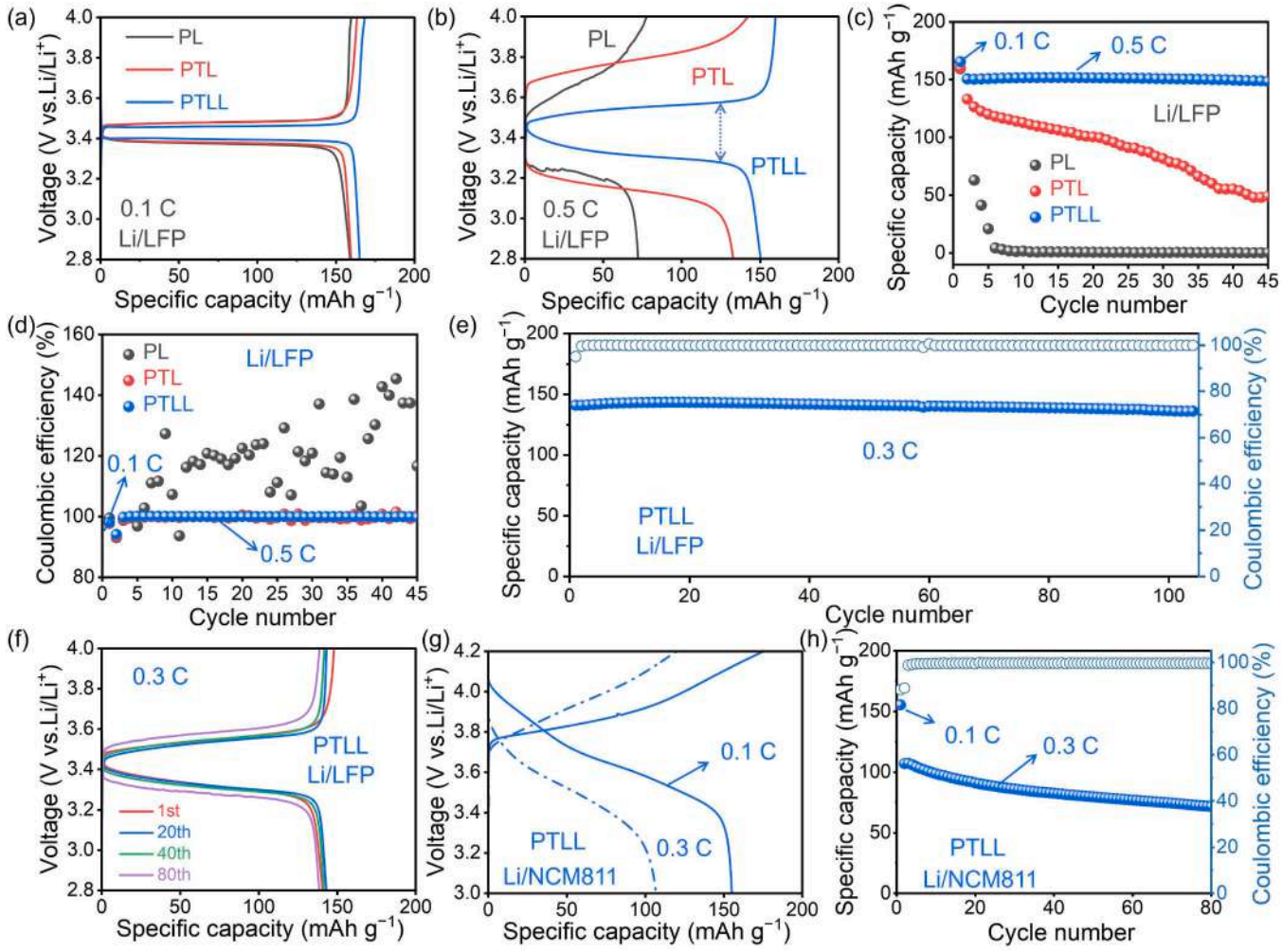


Fig. 5. Galvanostatic discharge/charge profiles of Li/LFP cells with various electrolytes at (a) 0.1 C and (b) 0.5 C at 60 °C. (c) Cycling performance and (d) Coulombic efficiency of Li/LFP cells with various electrolytes. (e) Long cycling performance and (f) galvanostatic discharge/charge profiles of Li/PTLL/LFP cell at 60 °C. (g) Galvanostatic discharge/charge profiles and (h) cycling performance of Li/PTLL/NCM811 cell at 60 °C.

This improvement is likely due to Lewis acid–base interactions between the surface of the LMS nanosheets and reactive groups (e.g., ether oxygen or terminal –OH) in PEO, which stabilize the polymer matrix against oxidation. These results confirm that the addition of TPU and LMS nanosheets effectively enhances the oxidative stability of PTLL electrolyte, rendering it more compatible with high-voltage cathodes such as NCM811 in solid-state lithium-metal batteries.

3.3. Plating/stripping behavior of symmetric Li/PTLL/Li cells

To investigate the lithium plating/stripping behavior of PL, PTL, and PTLL electrolytes, symmetric Li/Li cells were assembled and measured at 60 °C. As demonstrated in Fig. 4a, the PTLL based symmetric cell maintains stable voltage polarization for over 800 h at a current density of 0.1 mA cm^{-2} and an areal capacity of 0.1 mAh cm^{-2}, suggesting stable lithium deposition and stripping during cycling. PTLL electrolyte shows a stable polarization voltage of 0.25 V, which is smaller than that of PTL-based cell (0.26 V, Fig. 4b). However, the PTL symmetric cell shows gradually increased voltage after 600 h and a rapidly decreased voltage after 730 h, which is attributed to the uneven lithium deposition during cycling and thus formation of lithium dendrites. Interestingly, symmetrical Li cell with PL electrolyte exhibits the smallest polarization voltage of < 0.05 V when compared with PTLL and PTL cells (Fig. 4c), which is due to the thickness difference between PL electrolyte and the other two electrolytes. However, this PL-based cell shows short circuit after 694 h because of the uneven lithium deposition and poor mechanical strength, leading to lithium dendrite growth. Based on the above results, the incorporation of LMS nanosheets not only facilitates Li^+ dissociation and transport but also likely contributes to stabilizing lithium metal because of the improve mechanical strength of robust PTLL electrolyte. Additionally, PTLL symmetric cell shows a higher critical current density of 0.2 mA cm^{-2} than that of PTL and PL electrolytes (Fig. S9), which further indicates the enhanced capability of mitigating lithium dendrite growth and thus stabilizing lithium metal of PTLL electrolyte.

3.4. Electrochemical performance of solid-state Li/PTLL/LFP and Li/PTLL/NCM811 cells

To further examine the application of PTLL electrolyte in solid-state lithium metal batteries, we assembled Li/PTLL/LFP cells and measured their cycling performances at 60 °C. As illustrated in Fig. 5a, the Li/LFP cell with PTLL electrolyte deliver a higher specific capacity of 165.5 mAh g^{-1} at 0.1 C when compared with PL (159.4 mAh g^{-1}) and PTL (160.0 mAh g^{-1}) electrolytes. However, when tested at 0.5 C, the PTLL-based Li/LFP cell still exhibits a higher specific capacity with much lower overpotential when compared with the PTL- and PL-based cells (Fig. 5b). This result is mainly caused by the improved ionic conductivity of PTLL electrolyte, leading to good utilization of active material and fast ion transport in Li/LFP cell. Moreover, the Li/PTLL/LFP cell

demonstrates a high and reversible specific capacity > 150 mAh g^{-1} at 0.5 C with a higher Coulombic efficiency (>99.8 %) after 45 cycles, significantly surpassing the specific capacities achieved by PTL- and PL-based cells (Fig. 5c and d). The incorporation of TPU and LMS nanosheets enhances the mechanical strength of PTLL electrolyte, effectively stabilizing lithium metal and thus contributing to the improved cycling stability at high rates. Additionally, the Li/PTLL/LFP cell delivers much improved rate capability when compared with the PTL- and PL-based cells (Fig. S10), indicating enhanced redox reaction kinetics in Li/LFP cell because of the promoted Li^+ mobility of PTLL electrolyte. As a result, the PTLL cell shows good cycling performance over 105 cycles at 0.3 C with a capacity retention of ~97 % (Fig. 5e and f). When tested at 30 °C, Li/PTLL/LFP cell delivers a specific capacity of 102.6 mAh g^{-1} at 0.05 C with stable cyclability over 50 cycles at 0.1 C (Fig. S11). However, the achieved capacity of Li/PTLL/LFP cell at 30 °C remains lower than its theoretical or elevated-temperature performance, which is probably due tot the kinetic limitations at the electrode–electrolyte. Moreover, the PTLL-based full cell with graphite as anode and LFP as cathode shows a specific capacity of 98.1 mAh g^{-1} at 0.01 C and can be cycled for 20 cycles at 0.1 C (Fig. S12), suggesting the potential application of PTLL electrolyte in practical batteries. Furthermore, the Li/PTLL/NCM811 cell exhibits a high initial specific capacity of 155.4 mAh g^{-1} and 107.0 mAh g^{-1} at 0.1 C and 0.3 C, respectively (Fig. 5g and h), suggesting promising application of PTLL electrolyte for solid-state lithium metal batteries using high-voltage cathodes.

4. Conclusion

In summary, we have successfully developed a high-performance composite electrolyte by incorporating thermoplastic polyurethane and lithium magnesium silicate into a PEO-based matrix (denoted as PTLL). The PTLL electrolyte exhibits much improved ionic conductivity and a higher lithium-ion transference number when compared with PEO-based electrolyte. These enhancements are attributed to the effective suppression of polymer crystallization and the Lewis acid-base interactions among lithium magnesium silicate, polymer chains, and lithium salt anions. These synergistic effects collectively facilitate Li^+ dissociation and enhance ion transport within PTLL electrolyte. Additionally, the robust PTLL electrolyte demonstrates much enhanced thermal stability and possesses an improved oxidation onset voltage above than that of conventional PEO electrolyte. The PTLL-based symmetrical lithium cell demonstrates good cycling stability up to 800 h with stable polarization voltage, indicating good compatibility of PTLL with lithium metal. As a result, the PTLL-based Li/LFP cell exhibits much better cyclability with a higher average Coulombic efficiency > 99.8 % at 60 °C when compared with conventional PEO electrolyte. Moreover, when applied in Li/NCM811 cell, the PTLL electrolyte enables good utilization of active material with high reversibility. This work provides a promising application of functional silicate fillers for advanced composite electrolytes towards high-performance solid-state lithium metal batteries.

CRediT authorship contribution statement

Xuemeng Gan: Methodology, Investigation, Formal analysis. **Qilin He:** Investigation, Formal analysis. **Xiaojie Zheng:** Investigation, Formal analysis. **He Lin:** Investigation, Formal analysis. **Xiaoping Wang:** Data curation. **Qiao Lin:** Investigation. **Liangjie Gu:** Data curation. **Qingsong Zhang:** Writing – review & editing, Supervision. **Weiqing Yang:** Writing – review & editing, Supervision. **Panpan Dong:** Writing – review & editing, Writing – original draft, Supervision, Investigation, Conceptualization. **Shangzhang Yu:** Methodology, Investigation, Formal analysis, Data curation.

Declaration of Competing Interest

The authors declare that they have no known competing financial interests or personal relationships that could have appeared to influence the work reported in this paper.

Acknowledgements

This work was supported by the Fundamental Research Funds for the Central Universities (No. 2682024CX059), Start-up Research Funding of Southwest Jiaotong University (No. 2682024KJ003), Postdoctoral Fellowship Program of China Postdoctoral Science Foundation (No. GZC20241407) and Sichuan Science and Technology Program (No. 2025ZNSFSC1413).

Appendix A. Supporting information

Supplementary data associated with this article can be found in the online version at doi:10.1016/j.jallcom.2026.186613.

References

[1] E. Pomerantseva, F. Bonaccorso, X. Feng, Y. Cui, Y. Gogotsi, Energy storage: the future enabled by nanomaterials, Science 366 (6468) (2019) eaan8285.
[2] N. Nitta, F. Wu, J.T. Lee, G. Yushin, Li-ion battery materials: present and future, Mater. Today 18 (5) (2015) 252–264.
[3] T. Wulandari, D. Fawcett, S.B. Majumder, G.E.J. Poinern, Lithium-based batteries, history, current status, challenges, and future perspectives, Battery Energy 2 (6) (2023) 20230030.
[4] Q. Zhao, S. Stalin, C.-Z. Zhao, L.A. Archer, Designing solid-state electrolytes for safe, energy-dense batteries, Nat. Rev. Mater. 5 (3) (2020) 229–252.
[5] P. Dong, Y. Cha, X. Zhang, J. Zamora, M.-K. Song, Poly(ethylene) oxide electrolytes for all-solid-state lithium batteries using microsized silicon/carbon anodes with enhanced rate capability and cyclability, ACS Appl. Mater. Interfaces 16 (31) (2024) 41018–41026.
[6] Z. Wang, J. Liu, M. Wang, X. Shen, T. Qian, C. Yan, Toward safer solid-state lithium metal batteries: a review, Nanoscale Adv. 2 (5) (2020) 1828–1836.
[7] Y. Zheng, Y. Yao, J. Ou, M. Li, D. Luo, H. Dou, Z. Li, K. Amine, A. Yu, Z. Chen, A review of composite solid-state electrolytes for lithium batteries: fundamentals, key materials and advanced structures, Chem. Soc. Rev. 49 (23) (2020) 8790–8839.
[8] D. Zhou, D. Shanmukaraj, A. Tkacheva, M. Armand, G. Wang, Polymer electrolytes for lithium-based batteries: advances and prospects, Chem 5 (9) (2019) 2326–2352.
[9] C. Tang, L. Yu, Q. Jiang, R. Gu, Y. Zhang, Z. Liu, W. Cai, H. Wu, Y. Zhang, M. Yao, Polymer-based electrolyte for lithium-based high-energy-density and safe energy storages devices: strategy and mechanisms, Renewables 2 (5) (2024) 297–340.
[10] J.C. Bachman, S. Muy, A. Grimaud, H.-H. Chang, N. Pour, S.F. Lux, O. Paschos, F. Maglia, S. Lupart, P. Lamp, L. Giordano, Y. Shao-Horn, Inorganic solid-state electrolytes for lithium batteries: mechanisms and properties governing ion conduction, Chem. Rev. 116 (1) (2016) 140–162.
[11] C. Liao, C. Yu, S. Chen, C. Wei, Z. Wu, S. Chen, Z. Jiang, S. Cheng, J. Xie, Mitigation of the instability of ultrafast Li-ion conductor Li6.6Si0.6Sb0.4S5I enables high-performance all-solid-state batteries, Renewables 1 (2) (2023) 266–276.
[12] Z. Huang, W. Sun, S. He, H. Hu, X. Li, K. Huang, Z. Yan, G. Guo, Y. Lei, L. Yang, J. Huang, G. Wang, Y. Liang, G. Xu, X. Wu, Elucidating and optimizing i occupation in lithium argyrodite solid electrolytes for advanced all-solid-state Li metal batteries, Exploration 5 (5) (2025) 20240050.
[13] L.-Z. Fan, H. He, C.-W. Nan, Tailoring inorganic–polymer composites for the mass production of solid-state batteries, Nat. Rev. Mater. 6 (11) (2021) 1003–1019.
[14] Q. Wang, Y. Zhou, X. Wang, H. Guo, S. Gong, Z. Yao, F. Wu, J. Wang, S. Ganapathy, X. Bai, B. Li, C. Zhao, J. Janek, M. Wagemaker, Designing lithium halide solid electrolytes, Nat. Commun. 15 (1) (2024) 1050.
[15] X. Xia, Z.-Q. Zhang, Q. Wen, P.-Y. Li, D.-H. Le, Z.-Y. Wang, P.-P. Dong, G.-D. Ren, J.-C. Zheng, Metal-organic-framework-based solid-state electrolytes for high-performance lithium metal batteries: Recent advances and prospects, Chin. Chem. Lett. (2025) 111653.
[16] X. Lu, Y. Wang, X. Xu, B. Yan, T. Wu, L. Lu, Polymer-Based Solid-State Electrolytes for High-Energy-Density Lithium-Ion Batteries – Review, Adv. Energy Mater. 13 (38) (2023) 2301746.
[17] Z. Xue, D. He, X. Xie, Poly(ethylene oxide)-based electrolytes for lithium-ion batteries, J. Mater. Chem. A 3 (38) (2015) 19218–19253.
[18] Y. Song, M. Su, H. Xiang, J. Kang, W. Yu, Z. Peng, H. Wang, B. Cheng, N. Deng, W. Kang, PEO-Based Solid-State Polymer Electrolytes for Wide-Temperature Solid-State Lithium Metal Batteries, Small 21 (3) (2025) 2408045.
[19] P. Dong, X. Zhang, K.S. Han, Y. Cha, M.-K. Song, Deep eutectic solvent-based polymer electrolyte for solid-state lithium metal batteries, J. Energy Chem. 70 (2022) 363–372.

[20] S. Huo, L. Sheng, W. Xue, L. Wang, H. Xu, H. Zhang, X. He, Challenges of polymer electrolyte with wide electrochemical window for high energy solid-state lithium batteries, InfoMat 5 (3) (2023) e12394.
[21] Q. Han, S. Wang, W. Kong, W. Ren, Y. Liu, H. Wang, Realizing compatibility of high voltage cathode and poly (ethylene oxide) electrolyte in all-solid-state lithium batteries by bilayer electrolyte design, Chem. Eng. J. 454 (2023) 140104.
[22] J. Feng, L. Wang, Y. Chen, P. Wang, H. Zhang, X. He, PEO based polymer-ceramic hybrid solid electrolytes: a review, Nano Converg. 8 (1) (2021) 2.
[23] M.U. Javed, S. Muhammad, Z. Wang, J. Li, X. Wu, A. Chukwuka, Y. Zhang, K. Wang, B. Guo, Metal-Organic Framework/Polymer Composites for Solid State Electrolytes-A Critical Review, J. Power Sources 640 (2025) 236720.
[24] Y.-J. Lim, Y.-H. An, N.-J. Jo, Polystyrene-Al2O3 composite solid polymer electrolyte for lithium secondary battery, Nanoscale Res. Lett. 7 (1) (2012) 19.
[25] C. Wang, T. Yang, W. Zhang, H. Huang, Y. Gan, Y. Xia, X. He, J. Zhang, Hydrogen bonding enhanced SiO2/PEO composite electrolytes for solid-state lithium batteries, J. Mater. Chem. A 10 (7) (2022) 3400–3408.
[26] X. Guo, R.-Z. Yuan, On the grain boundaries of ZrO2-based solid electrolyte, Solid State Ion. 80 (1) (1995) 159–166.
[27] J. Yang, Y. Jia, Z. Yao, Study on the lithium solid electrolytes of Li 3N-Li 3Bi-LiCl ternary system — 2Li 3Bi · 3LiCl lithium solid electrolyte, Solid State Ion. 96 (3) (1997) 215–218.
[28] J. Seo, M. Nasir, H.J. Park, Lithium-Ion Conduction Pathways in LLZO-PEO Composite Solid Electrolytes, ACS Appl. Energy Mater. 8 (3) (2025) 1518–1525.
[29] T. Duan, H. Cheng, Y. Liu, Q. Sun, W. Nie, X. Lu, P. Dong, M.-K. Song, A multifunctional Janus layer for LLZTO/PEO composite electrolyte with enhanced interfacial stability in solid-state lithium metal batteries, Energy Storage Mater. 65 (2024) 103091.
[30] H.-T. Li, G.-C. Wang, Z.-H. Kang, Y. Zheng, N.-N. Wu, X. Tao, High-voltage poly (ethylene oxide) all-solid-state lithium batteries enabled by high-concentration interfacial layer, Rare Met. 44 (10) (2025) 7136–7146.
[31] L. He, W.-H. Liang, J.-H. Cao, D.-Y. Wu, PI-LATP-PEO Electrolyte with High Safety Performance in Solid-State Lithium Metal Batteries, ACS Appl. Energy Mater. 5 (4) (2022) 5277–5286.
[32] G. Lu, H. Wei, C. Shen, F. Zhou, M. Zhang, Y. Chen, H. Jin, J. Li, G. Chen, J. Wang, S. Wang, Bifunctional MOF Doped PEO Composite Electrolyte for Long-Life Cycle Solid Lithium Ion Battery, ACS Appl. Mater. Interfaces 14 (40) (2022) 45476–45483.
[33] Z. Zhang, L. Tian, H. Zhang, H. Xu, P. Dong, Y. Zhang, D. Long, Hexagonal Rodlike Cu-MOF-74-Derived Filler-Reinforced Composite Polymer Electrolyte for High-Performance Solid-State Lithium Batteries, ACS Appl. Energy Mater. 5 (1) (2022) 1095–1105.
[34] J. Chen, S. Han, PEO-based solid-state electrolyte modified by cationic covalent organic frameworks enabling high-performance all-solid-state Li metal and graphite anode batteries, Chem. Eng. J. 470 (2023) 144150.
[35] W. Tang, S. Tang, C. Zhang, Q. Ma, Q. Xiang, Y.-W. Yang, J. Luo, Simultaneously Enhancing the Thermal Stability, Mechanical Modulus, and Electrochemical Performance of Solid Polymer Electrolytes by Incorporating 2D Sheets, Adv. Energy Mater. 8 (24) (2018) 1800866.
[36] J. Song, Y. Xu, Y. Zhou, P. Wang, H. Feng, J. Yang, F. Zhuge, Q. Tan, Incorporating 2D γ-Al2O3 nanosheets into the flexible PEO-based solid electrolyte for lithium metal batteries, Electrochim. Acta 437 (2023) 141504.
[37] M. Lei, X. Wu, Y. Liu, K. Chen, J. Hu, C. Li, Polymer electrolytes reinforced by 2D fluorinated filler for all-solid-state Li-Fe-F conversion-type lithium metal batteries, Nano Res. 16 (6) (2023) 8469–8477.
[38] J. Li, W. Zheng, L. Zhu, H. Zhou, K. Zhang, Incorporating lithium magnesium silicate into PVDF-HFP based solid electrolyte to achieve advanced solid-state lithium-ion batteries, J. Alloy. Compd. 960 (2023) 170640.
[39] Y. Zhang, J.-H. Li, M. Ge, Y.-H. Huang, H.-H. Xu, Transparent PVDF-based electrolyte enabled by lipophilic lithium magnesium silicate for solid-state lithium batteries, Rare Met. 43 (11) (2024) 5625–5636.
[40] C. Tao, M.-H. Gao, B.-H. Yin, B. Li, Y.-P. Huang, G. Xu, J.-J. Bao, A promising TPU/PEO blend polymer electrolyte for all-solid-state lithium ion batteries, Electrochim. Acta 257 (2017) 31–39.
[41] Y. Zhang, J. Yu, H. Shi, S. Wang, Y. Lv, Y. Zhang, Q. Yuan, J. Liang, T. Gao, R. Wei, X. Chen, L. Wang, Y. Yu, W. Liu, Fiber-reinforced ultrathin solid polymer electrolyte for solid-state lithium-metal batteries, Adv. Funct. Mater. 35 (25) (2025) 2421054.
[42] A.M. Pillai, R. Ghosh, A. Dey, K. Prajwal, A. Rajendra, A.K. Sharma, S. Sampath, Crystalline and amorphous PEO based ceramic coatings on AA6061: Nanoindentation and corrosion studies, Ceram. Int. 47 (10, Part B) (2021) 14707–14716.
[43] M. Zuo, Z. Bi, X. Guo, In-situ solidification of plastic interlayers enabling high-voltage solid lithium batteries with poly(ethylene oxide) based polymer electrolytes, Chem. Eng. J. 463 (2023) 142463.